KSCE Journal of Civil Engineering (2017) 21(3):734-745
DOI 10.1007/s12205-016-0867-9

Geotechnical Engineering
pISSN 1226-7988, eISSN 1976-3808
www.springer.com/12205

A Modified Elasto-plastic Model with Double Yield Surfaces and Considering Particle Breakage for the Settlement Analysis of High Rockfill Dams

Raksiri Sukkarak*, Pornthap Pramthawee, and Pornkasem Jongpradist*****

Received Octoer 15, 2015/Accepted May 15, 2016/Published Online June 15, 2016

Abstract

This paper improves the elasto-plastic model with double yield surfaces in the context of the hardening soil model for the simulation of the settlement behavior of high rockfill dams. The stress-dependent stiffness values (E_{50} and E_{oed} control the shear hardening and the cap yield surfaces, respectively) are modified to exhibit different degrees of evolution with changes in the stress state. A modification of Rowe's stress-dilatancy theory is proposed to account for the influence of particle breakage. Good quantitative agreement between simulated and measured stress-strain relationships can be achieved; in particular, the volumetric strain is much improved from the original model. The developed model is applied to predict the settlement of Nam Ngum 2, a 182 m high rockfill dam, during the construction stage, in conjunction with a three-Dimensional (3D) Finite Element (FE) analysis. The findings show that a good agreement between computed settlements and dam field monitoring data can be achieved.

Keywords: *double yield surfaces, stress-dependent stiffness, particle breakage, modified rowe's stress-dilatancy theory, high rockfill dam*

1. Introduction

Rockfill material is widely used in many geotechnical applications, especially rockfill dams. Rockfill dams have been increasingly constructed in recent years in many parts of the world because of their various advantages, such as their use of local materials, their inherent flexibility, their capacity for absorbing large amounts of seismic energy, their adaptability to various foundation conditions, and the fact that they are the lowest-cost type of dam to build. Currently, many construction projects involving high rockfill dams of over 200 m in height are underway. These projects require millions of cubic meters of rock-filled materials. To address economic and safety concerns in dam design, a number of researchers have investigated the behaviors of rockfill materials by conducting tests using large-scale apparatuses at high levels of pressure (Charles and Watts, 1980; Varadarajan *et al*., 2003; Varadarajan *et al*., 2006; Alonso *et al*., 2011; Xu *et al.*, 2012a). Based on these experimental results, rockfill materials have been found to exhibit nonlinearity in stress-strain-volumetric strain changes, stress dependence, shear dilatancy and particle breakage when subjected to compression or shear stresses.

The hyperbolic model developed by Duncan and Chang (1970) was first used to predict the stress-strain curves of rockfills in triaxial compression tests. The hyperbolic model is still commonly used in current practice, although this model cannot simulate the volumetric dilatancy of rockfills under shearing because it is based on the generalized Hooke's law (Xu and Song, 2009). Over the past decade, several constitutive models based on elasto-plastic theory have been established to achieve more realistic prediction of the responses of rockfill materials in terms of stress-strain-volumetric strain changes (e.g., Varadarajan *et al*., 2003&2006; Zhang *et al*., 2007; Xu and Song, 2009). Among these, the Hardening Soil (HS) model is one of the candidates used to characterize the behavior of rockfill materials. The HS model was formulated based on the theory of elasto-plasticity with double yield surfaces, introducing a yield cap, a stress-dependent stiffness and dilatancy. Loupasakis *et al*. (2009) and Araei (2014) have reported that these features endow simulations using the HS model with the ability to capture the behavior of rockfill materials with sufficient accuracy compared with experimental results. In recent years, the HS model has been implemented in rockfill dam stress-deformation analyses (Ozkuzukiran *et al*.,

*Ph.D. Candidate, Civil Engineering Dept., Faculty of Engineering, King Mongkut's University of Technology Thonburi, Thung Khru, Bangkok, Thailand (E-mail: sukkarak.r@gmail.com)
**Ph.D. Student, Civil Engineering Dept., Faculty of Engineering, King Mongkut's University of Technology Thonburi, Thung Khru, Bangkok, Thailand (E-mail: pornthap.kmutt@mail.kmutt.ac.th)
***Associate Professor, Civil Engineering Dept., Faculty of Engineering, King Mongkut's University of Technology Thonburi, Thung Khru, Bangkok, Thailand (Corresponding Author, E-mail: pornkasem.jon@kmutt.ac.th)

2006; Soroush and Araei, 2006; Kohgo *et al*., 2010; Mahabad *et al*., 2014). Although the simulation results satisfactorily reproduce the monitoring data, the back-calculation method has been applied to obtain the parameters.

Although many essential features of rockfills have been included in the HS model (i.e., nonlinearity, stress-dependent stiffness and shear dilatancy), the model was originally developed for soils (i.e., sands and clays) (Schanz *et al*., 1999). The main considerations for model development and parameter determination were thus derived from and are relevant to the behavior of soils. To better adapt the model for application to rockfills, several additional features of which still have not yet been considered, further development is necessary. The features yet to be satisfactorily incorporated into the model include the significant changes in volume due to compression under high confining pressures (Varadarajan *et al.*, 2003&2006) and particle breakage (Salim and Indraratna, 2004; Liu and Zou, 2013; Xiao *et al.*, 2014). The capability of simulating volume changes has a strong influence on predictions of the deformations of rockfill dams, which are very important for face slab safety assessment during the design process.

Numerous investigators have indicated that the stress-strain-volumetric strain change of rockfill materials is influenced by particle breakage phenomena (Marsal, 1967; Lade *et al*., 1996; Salim and Indraratna, 2004; Liu and Zou, 2013). Several methods have been proposed to quantify the amount of particle breakage (Marsal, 1967; Lee and Farhoomand, 1967; Hardin, 1985). Recently, Einav (2007) developed a particle breakage factor based on fractal theory. It may be possible to describe the evolution of particle breakage based on the evolution of the energy input to the specimen (Miura and O-hara, 1979; Hardin 1987).

The objectives of this study are to further develop the constitutive model in the context of the HS model for simulating the behavior of rockfill materials and to implement the improved model in a numerical analysis tool for the deformation analysis of high rockfill dams. In particular, we focus on the stress-dependent stiffness values (E_{50} and E_{oed}, which control the primary deviatoric loading in triaxial tests and the primary oedometer loading, respectively), which are considered separately, and we take particle breakage into account. The comprehensive testing results of Nam Ngum 2 rockfill materials, which have been well documented (including triaxial and oedometer tests), are used to investigate the significance of the effects of the stress-dependent stiffness and particle breakage. A modification to Rowe's dilatancy equation is introduced in the current work to account for particle breakage. The particle breakage index (B_g) developed by Einav (2007) is adopted to define the amount of particle breakage in the modified model. Then, the modified model is applied to predict the settlement of the Nam Ngum 2 Concrete Face Rockfill Dam (CFRD) during the construction stage via a three-Dimensional (3D) finite element analysis. To verify the performance of the improved model, comparisons between the predicted results and the field monitoring data are provided in the latter part of this article.

2. Assumptions and Preliminary Investigation of the Simulation Capability of the Original Model for Rockfill Materials

As previously mentioned, the HS model was developed for soils under conditions in which the considered stress level (such as the confining pressure in a triaxial test) is in the range of tens to a few hundreds of kPa. By contrast, the stresses considered in rockfill testing for high CFRDs range from several hundreds of kPa to a few MPa.

In the HS model (hereafter called the original model), the stiffnesses for primary deviatoric loading and primary compression are controlled by E_{50} and E_{oed}, respectively, as shown in Fig. 1. Both of these quantities vary with the evolution of the stress state in a power-law form (refer to parameter m in the figure) with respect to the initial input parameters E_{50} and E_{oed} determined at the referenced stress. Based on previously reported test results for soils (e.g., Surasak *et al*., 2012 for clays), it has been confirmed that the power parameter m takes approximately the same values in the stress states corresponding to both triaxial and oedometer tests and that these values lie in the range of 0.8-1. However, no study has yet discussed the validity of these stiffness moduli for rockfill materials because very few authors have reported data from both triaxial and oedometer tests. The power parameter m is commonly obtained from the results of triaxial tests and used for both E_{50} and E_{oed}, as follows:

$$E_{50} = E_{50}^{ref}\left(\frac{c\cos\varphi - \sigma_3'\sin\varphi}{c\cos\varphi + p^{ref}\sin\varphi}\right)^m \tag{1}$$

$$E_{oed} = E_{oed}^{ref}\left(\frac{c\cos\varphi - \frac{\sigma_3'}{K_0^{nc}}\sin\varphi}{c\cos\varphi + p^{ref}\sin\varphi}\right)^m \tag{2}$$

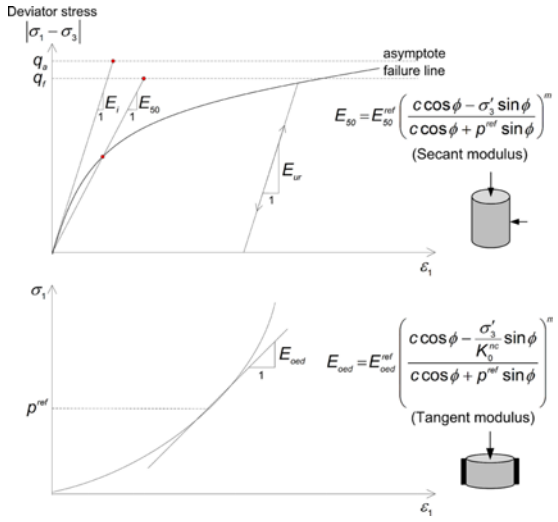

Fig. 1. The Stress-strain Relation: (a) in Primary Loading for Standard Drained Triaxial Test, (b) Definition of the Stiffness Modulus from Oedometer Test E_{oed}

This implies that the original model assumes the same degree of evolution with the stress state (m) for both E_{oed} and E_{50}. In our preliminary investigation using model parameters directly obtained from a previous recommendation (Schanz *et al.*, 1999), the original model satisfactorily reproduced the test results only in terms of the deviator stress. Rockfill exhibits deformations in terms of volumetric strain that are much larger than those indicated by the simulations. Further investigation was then conducted by determining the model parameters in accordance with their physical meanings from the original model to verify our hypothesis that different parameters m for the deviatoric stress state (defined as m_{tri}) and the compression stress state (defined as m_{oed}) should be adopted for rockfill materials.

The experimental data (including data from triaxial and oedometer tests) used in this research were based on those for the construction of the Nam Ngum 2 dam by the Institute of Water Resources and Hydropower Research (IWHR) and the Asian Institute of Technology (AIT). The rockfills in this project consisted of blended rockfill materials containing sandstone and siltstone (six types) (IWHR, 2007). The confining pressures were varied from 0.5 to 2 MPa in the triaxial tests, whereas a maximum vertical stress of 3.2 MPa was applied in the oedometer tests. The rockfill samples were prepared by controlling the compaction to obtain a dry unit weight of 21.0-21.5 kN/m^3. During the preparation of the test samples, a combination of the Equivalent Quantity Replacement Method (EQRM) and the Similar Particle Distribution Method (SPDM) was utilized to scale down the original materials. The methods used were also in accordance with the Specification of Soil Test SL237-1999 (NJHRI, 1999).

Figs. 2(a) and 2(b) show log-log plots of $\left(E_{50}-\frac{\sigma_3'}{p^{ref}}\right)$ and $\left(E_{oed}-\frac{\sigma_1'}{p^{ref}}\right)$, respectively. It was found that the slope values m_{oed} are lower than the m_{tri} values. For future reference, the relationship of the aforementioned data can be estimated using the following linear function (see Fig. 2(c)):

$$m_{oed} = 0.651 m_{tri} \tag{3}$$

The findings of this preliminary investigation confirm our hypothesis that the stress-dependent compression under high levels of stress is likely the key factor controlling the volume behavior of rockfills. Therefore, not only the stiffness values for primary deviatoric loading and primary compression but also their degree of stress dependence must be separately considered in the model, as described in the next section.

Rowe's dilatancy equation, as used in the original model, implies that the rate of post-peak volume change remains constant. Figure 3 illustrates an example of such an evolution of $\sin\varphi_m/\sin\varphi_{cv}$ and the change in the volumetric strain ε_V of rockfill 3A (to be explained later). As seen from this figure, the rockfill exhibits higher contraction at high confining pressures (2 MPa). When the confining pressure is low (1.0 MPa), the evolution of $\sin\varphi_m/\sin\varphi_{cv}$ is obviously faster than that in the case of a high confining pressure. Rockfills undergo volumetric dilation after the peak state; however,

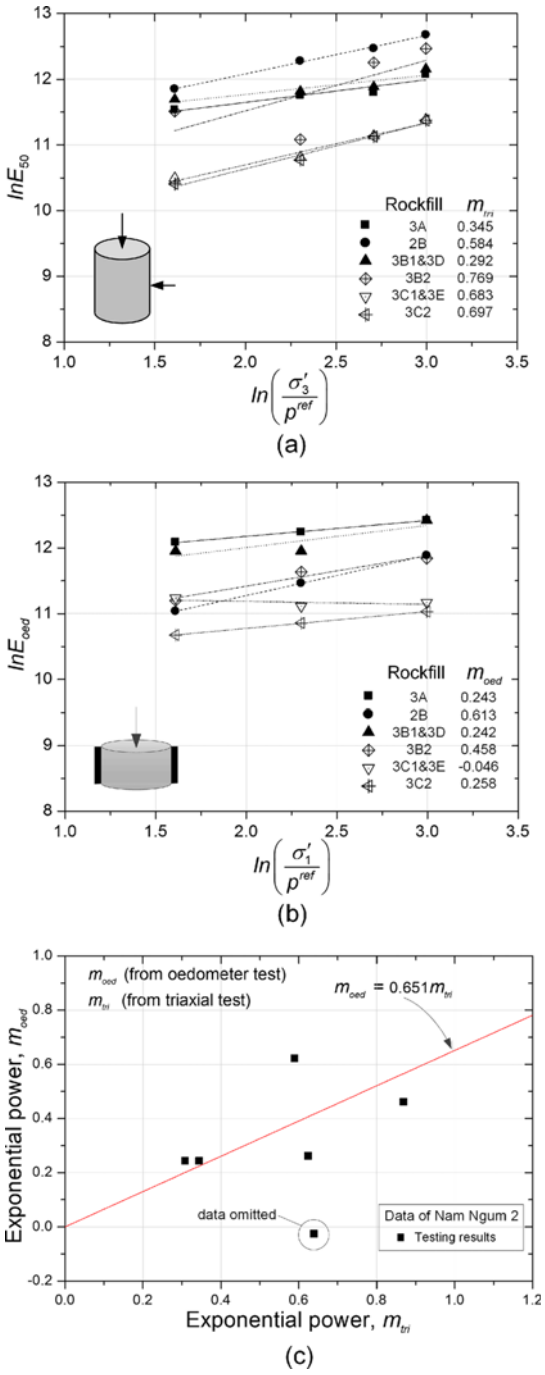

Fig. 2. Stiffness Dependences Observed for Nam Ngum 2 Rockfill Materials: (a) Variation of E_{50} with Confining Pressure, (b) Variation of E_{oed} with Confining Pressure, (c) Relation between m_{oed} and m_{tri}

the volumetric strain rate changes. This may be attributed to the occurrence of particle breakage during compression or shearing, which is an important feature of rockfill materials. As indicated by laboratory investigations, the transference of high stress concentrations among rockfill particles may result in some level of particle breakage (e.g., Xiao *et al.*, 2014), which cannot be neglected. In the oedometer tests considered in this study, the particle gradation of the tested rockfills was quantified both

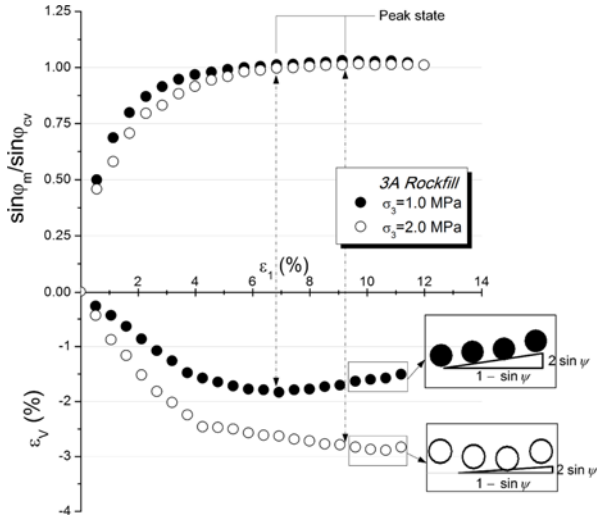

Fig. 3. 3A Rockfill Material Observed at Various Confining Pressures

before and after testing (the results will be shown later). The results indicated changes in the particle gradation of all types of rockfill.

3. Modification and framework of the constitutive model

3.1 Hyperbolic relationship for a standard drained triaxial test

In the hyperbolic model developed by Duncan & Chang (1970), a hyperbolic function is used to express the stress-strain relations of the original model under primary triaxial loading. Here, ε_1 is the vertical strain and q is the deviatoric stress. Based on a standard drained triaxial test, the relationship between ε_1 and q can be expressed as follows:

$$-\varepsilon_1 = \frac{1}{E_i}\frac{q}{1-q/q_a} \quad \text{for } q < q_f \tag{4}$$

where q_a and E_i are the asymptotic value and the initial stiffness, respectively, whereas E_i is related to E_{50} by the following expression:

$$E_i = \frac{2E_{50}}{2-R_f} \tag{5}$$

3.2 Shear Yield Surface

The shear hardening yield function f is specified in the following form:

$$f = \bar{f} - \gamma^p \tag{6}$$

$$\bar{f} = \frac{2}{E_i}\frac{q}{1-q/q_a} - \frac{2q}{E_{ur}} \tag{7}$$

$$\gamma^p = -(2\varepsilon_1^p - \varepsilon_v^p) \approx -2\varepsilon_1^p \tag{8}$$

Here, $\bar{f}$ and γ^p are the functions of stress and plastic strain, respectively. For hard soils, the volumetric changes in plastic strain (ε_v^p) tend to be relatively small, satisfying conditions that give rise to the approximation $\gamma^p \approx -2\varepsilon_1^p$.

It is assumed that the yield $\gamma^p = \bar{f}$ for the primary loading as:

$$\varepsilon_1^p \approx \frac{1}{2}\bar{f} = \frac{2}{E_i}\frac{q}{1-q/q_a} - \frac{q}{E_{ur}} \tag{9}$$

As the elastic parameters for both primary loading and unloading/reloading, E_{ur} is the elastic Young's modulus and υ_{ur} is the Poisson's ratio for unloading/reloading. The elastic strains considered for both primary loading and unloading/reloading are calculated as follows:

$$-\varepsilon_1^e = \frac{q}{E_{ur}} \tag{10}$$

$$-\varepsilon_2^e = -\varepsilon_3^e = -\upsilon_{ur}\frac{q}{E_{ur}} \tag{11}$$

3.3 Cap yield surface

A second yield surface (the cap yield surface) is introduced to close the elastic region under isotropic compression. In the original model, the shear yield surface is primarily controlled by the stiffness modulus from the triaxial test, whereas the cap yield surface is largely controlled by the stiffness modulus from the oedometer test. Note that the magnitude of the plastic strain related to the shear yield surface is largely controlled by E_{50}. For the cap yield surface, the variable that controls the magnitude of the plastic strain is E_{oed}. The yield function for the yield cap is expressed as follows:

$$f^c = \frac{\tilde{q}^2}{\alpha^2} + p'^2 - p_p^2 \tag{12}$$

where α is an auxiliary model parameter that is related to K_0^{nc}.

For an associated flow rule in plasticity, a plastic potential function g^c is defined that is identical to the yield function f^c as follows:

$$g^c = f^c \tag{13}$$

The magnitude of the yield cap is determined by the isotropic pre-consolidation stress p_p. The hardening relating p_p to the volumetric cap strain ε_v^{pv} is

$$\varepsilon_v^{pv} = \frac{\beta}{1-m}\left(\frac{p_p}{p^{ref}}\right)^{1-m} \tag{14}$$

3.4 Stress-dependent Stiffness Following a Power Law

The actual stiffness moduli are updated in accordance with the current stress level, which is controlled by a model constant (the power parameter). To allow for different degrees of evolution of the stress-dependent stiffness, the model constant m_{oed} must be defined separately; it is denoted by n in this study:

$$E_{oed} = E_{oed}^{ref}\left(\frac{c\cos\varphi - \frac{\sigma_3'}{K_0^{nc}}\sin\varphi}{c\cos\varphi + p^{ref}\sin\varphi}\right)^n \tag{15}$$

The stress-dependent stiffness modulus in the cases of unloading and reloading stress paths can be expressed as follows:

$$E_{ur} = E_{ur}^{ref}\left(\frac{c\cos\varphi - \sigma_3'\sin\varphi}{c\cos\varphi + p^{ref}\sin\varphi}\right)^m \tag{16}$$

3.5 Plastic Strain in the Mobilized Friction Angle

The increment in plastic strain can be determined based on the relationship between $\dot{\varepsilon}_v^p$ and $\dot{\gamma}^p$, and the flow rule is given as follows:

$$\dot{\varepsilon}_v^p = \sin\psi_m \dot{\gamma}^p \tag{17}$$

According to Rowe's original stress-dilatancy theory (Rowe, 1962), the dilatancy equation can be written as follows:

$$\sin\psi_m = \frac{\sin\varphi_m - \sin\varphi_{cv}}{1 - \sin\varphi_m \sin\varphi_{cv}} \tag{18}$$

where ψ_m is the mobilized dilatancy angle and φ_{cv} and φ_m are the critical-state friction angle and the mobilized friction angle, respectively. φ_{cv} and φ_m may be defined as follows:

$$\sin\varphi_{cv} = \frac{\sin\varphi - \sin\psi}{1 - \sin\varphi\sin\psi} \tag{19}$$

$$\sin\varphi_m = \frac{\sigma_1' - \sigma_3'}{\sigma_1' + \sigma_3' - 2c\cot\varphi} \tag{20}$$

It can be observed that volumetric dilation occurs under high-stress-ratio conditions, $\varphi_m > \varphi_{cv}$.

3.6 Modification to Rowe's Stress-dilatancy Equation

It is well known that particle breakage commonly occurs when rockfill materials are subjected to compression or shearing, even at low confining pressures. Numerous investigators have indicated that the dilatancy behavior tends to decrease with an increasing degree of particle breakage (Marsal, 1967; Lade *et al*., 1996; Salim and Indraratna, 2004; Liu and Zou, 2013). In previous works, the volumetric strain response of rockfill material under shearing has been correlated with the degree of particle breakage, as identified in the use of state parameters based on the critical-state concept (Liu and Zou, 2013, Xiao *et al*., 2014). In this study, we propose a simplified method of considering the effect of particle breakage on the dilatancy of rockfill materials. For this purpose, a modification of Rowe's stress-dilatancy equation that incorporates particle breakage behavior is proposed in this study.

In Rowe's original dilatancy model, the mobilized dilation angle (ψ_m) is defined by the following equation:

$$\sin\psi_m = \frac{\sin\varphi_m - \sin\varphi_{cv}}{1 - \sin\varphi_m \sin\varphi_{cv}} \tag{21}$$

In this study, the evolution of the dilation angle with respect to the particle breakage variable is defined as $\psi_{m,bg}$. The introduced $\psi_{m,bg}$ is defined by the following relation:

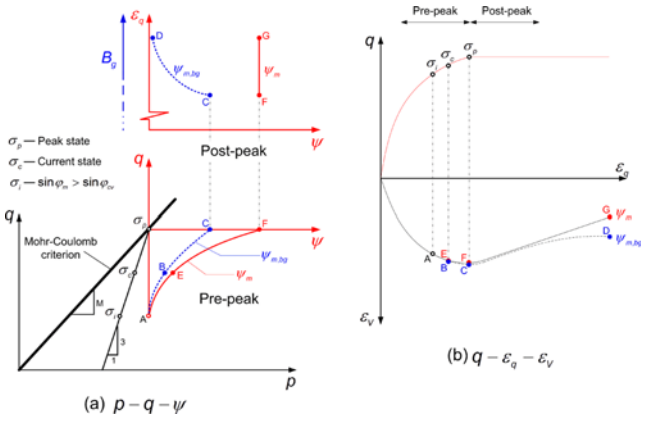

Fig. 4. Evolution of the Dilation Angle in the Original and Modified Rowe Stress-dilatancy Theories: (a) $p-q-\psi$, (b) $q-\varepsilon_q-\varepsilon_V$

$$\sin\psi_{m,bg} = \frac{(\sin\varphi_m - \sin\varphi_{cv})\cdot(1 - B_g^{\lambda})}{1 - \sin\varphi_m \sin\varphi_{cv}} \tag{22}$$

where $\psi_{m,bg}$ is the modified mobilized dilatancy angle, B_g is the particle breakage index, and λ is the power-law parameter for breakage.

Figures 4(a)-(b) show how the mobilized dilation angle ψ_m and the volumetric strain ε_V develop along the stress path of a drained triaxial test. The figure provides a comparison between the general principle of the Original Rowe (OR) stress-dilatancy theory and the Modified Rowe (MR) stress-dilatancy theory incorporating particle breakage. A volumetric contraction response occurs during the early stage of shearing, as displayed in Fig. 4(b). The mobilized dilation angle (ψ_m) initially has a value of zero, until $\sin\varphi_m$ grows greater than $\sin\varphi_{cv}$ ($\sin\varphi_m > \sin\varphi_{cv}$). Hence, the first point to note (point A) is the onset point of a non-zero ψ_m($\psi_m > 0$). For the OR theory (path A-E-F), ψ_m increases during the evolution of the stress state, as seen from the red solid line (see Fig. 4(a)). By contrast, the evolution of the mobilized dilation angle with respect to the particle breakage variable (path A-B-C) is represented by the blue dashed line. Simultaneously, $\psi_{m,bg}$ is suppressed by the effect of particle breakage, as depicted by the blue dashed line. At this state (pre-peak), considering the volumetric strain response, there is a small difference between the OR and MR (see Fig. 4(b)). At post-peak state, for the OR case (F-G), the volumetric strain response changes with a constant ratio of$\Delta\varepsilon_V/\Delta\varepsilon_q$ because of the full mobilization of ψ_m($\psi_m = \psi_{input}$), whereas for the MR case, $\psi_{m,bg}$ vanishes gradually with the evolution of the particle breakage variable B_g. The ratio $\Delta\varepsilon_V/\Delta\varepsilon_q$ tends to decrease with an increase in particle breakage B_g, and it reaches zero in the final state, as has been widely discussed in past publications (Salim and Indraratna, 2004; Liu and Zou, 2013; Xiao *et al*., 2014).

To quantify the particle breakage, the modified definition proposed by Einav (2007) is adopted in this study to represent the change in the particle distribution, as shown in Fig. 5:

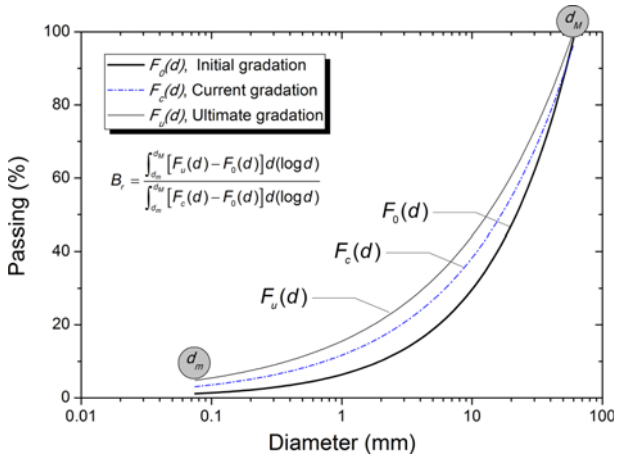

Fig. 5. Definition of the Particle Breakage Index (modified following Einav (2007))

$$B_g = \frac{\int_{d_m}^{d_M}[F_u(d)-F_0(d)]d(\log d)}{\int_{d_m}^{d_M}[F_c(d)-F_0(d)]d(\log d)} \tag{23}$$

where F_0, F_c and F_u are the initial, current and ultimate gradation curves, respectively. These curves are defined as follows:

$$F_0(d) = \left(\frac{d}{d_M}\right)^{3-\alpha_0} \tag{24}$$

$$F_c(d) = \left(\frac{d}{d_M}\right)^{3-\alpha_0} \tag{25}$$

$$F_u(d) = \left(\frac{d}{d_M}\right)^{3-\alpha_u} \tag{26}$$

where α_0, α_c and α_u are the fractal dimensions for the initial, current and ultimate gradation curves, respectively, and d, d_m and d_M are the particle diameter, minimum particle diameter and maximum particle diameter, respectively. α_0 and α_c can be determined by fitting the gradation curve before and after the test. For rockfill materials, a value of $\alpha_u = 2.7$ is generally used, as suggested by Yang and Juo (2001). The traditional theory of particle breakage evolution is related to the plastic work W_p and can be defined in terms of a hyperbolic function (see Fig. 6):

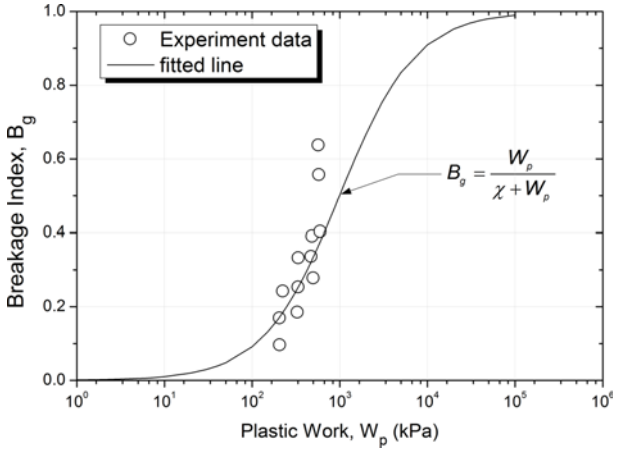

Fig. 6. Relationship between the Particle Breakage Index and the Plastic Work for the Rockfill Materials Considered in this Study

$$B_g = \frac{W_p}{\chi + W_p} \tag{27}$$

where W_p can be written in the following form:

$$W_p = \int p' d\varepsilon_v^p + q d\varepsilon_s^p \tag{28}$$

4. Determination and Calibration of Model Parameters

4.1 Failure Parameters in the Mohr-Coulomb Criterion

The values of c and φ can be obtained from the relationship between the deviator stress q and the effective mean stress p. For granular materials such as sand, gravel and rockfill, c is typically assumed to be a small value. A number of large-scale triaxial experiments have illustrated that the friction angle of a rockfill material is a function of the confining pressure, as described by the following equation:

$$\varphi = \varphi_0 - \Delta\varphi \log\left(\frac{\sigma_3'}{p_a}\right) \tag{29}$$

where p_a is the atmospheric pressure, φ_0 is the reference friction angle, and $\Delta\varphi$ is the reduction factor.

4.2 Stiffness Parameters

To determine the values of the stiffness parameters using the present model, it is necessary to define a reference stress p^{ref}. In this study, $p^{ref} = 100$ kPa is chosen. The triaxial-test stiffness modulus can be determined from the y intercept in $\log(\sigma^3/p^{ref})$ and $\log(E_{50})$ space, as depicted in Fig. 1(a). Here, the slope of the trend line of this relationship is the stress-dependence parameter of the stiffness (m). Likewise, the oedometer-test stiffness modulus can be determined from the y intercept in $\log(\sigma_1/p^{ref})$ and $\log(E_{oed})$ space (see Fig. 1(b)). The reference stiffness for elastic unloading/reloading E_{ur}^{ref} is generally set to $3E_{50}^{ref}$.

4.3 Advance Parameters

υ_{ur} is set to approximately 0.3. The value of K_0^{NC} can be obtained from Jaky's formula, $K_0^{NC} = 1 - \sin\varphi$. The failure ratio ($R_f$) should be smaller than 1. The overconsolidation ratio (OCR) is set equal to 1. Note that we also need to identify the constant model parameters; the following model parameters are used: p^{ref} = 100 kPa, c = 1 kPa, OCR = 1, $K_0^{NC} = 1 - \sin\varphi$ and $\upsilon_{ur} = 0.3$.

4.4 Breakage Parameters

Values of $\chi = 993$ and $\lambda = 0.268$ were obtained for the Nam Ngum 2 rockfill materials.

The constitutive model was implemented in a finite element analysis program using user-defined material subroutines, called 'UMAT,' for ABAQUS/Standard. The numerical formulation of the model implementation follows the guidelines suggested by

Table 1. Model Parameters for Nam Ngum 2 Rockfill Materials

Parameter	Zone					
	2B	3A	3B1&3D	3B2	3C1&3E	3C2
φ_0 (degree)	43.23	46.08	47.09	42.60	42	43.30
$\Delta\varphi$	1.16	2.59	2.99	2.55	2.45	3.95
ψ_0 (degree)	3.2	3.2	3.2	0.5	-5	-5
E_{50}^{ref} (MPa)	65	65	80	32	20	12
E_{oed}^{ref} (MPa)	50	52	55	24	17	10
m	0.45	0.34	0.29	0.69	0.68	0.70
n	0.25	0.24	0.14	0.42	0.32	0.26
R_f	0.74	0.75	0.78	0.82	0.68	0.65
Other	$E_{ur}^{ref}=3E_{50}^{ref}$, $p^{ref}=100$ kPa, $c=1$ kPa, $OCR=1$, $K_0^{NC}=1-\sin\varphi$, $\upsilon_{ur}=0.3$					
Breakage parameter	$\chi=993$, $\lambda=0.268$					

Dunne and Petrinic (2005). The verification process was conducted by comparing the simulated results obtained from ABAQUS using these subroutines to the experimental results. The parameters are listed in Table 1.

Figures 7(a)-(c) compare the predicted and experimental results in terms of the stress-strain-volumetric strain behavior of the Nam Ngum 2 rockfills of types 2B, 3A and 3C1, respectively. The experimental data are presented as symbols, and the predicted results are shown as solid lines. In terms of the deviator stress, the predicted results achieve highly satisfactory agreement with the test results. The peak deviator stress can be clearly found from the data sets of rockfills 2B and 3A. For the volumetric strain response, the predicted results are in good agreement with the test results in regard to both tendency and magnitude. For the evolution of the particle distribution for various confining pressures, the predicted results are also close to

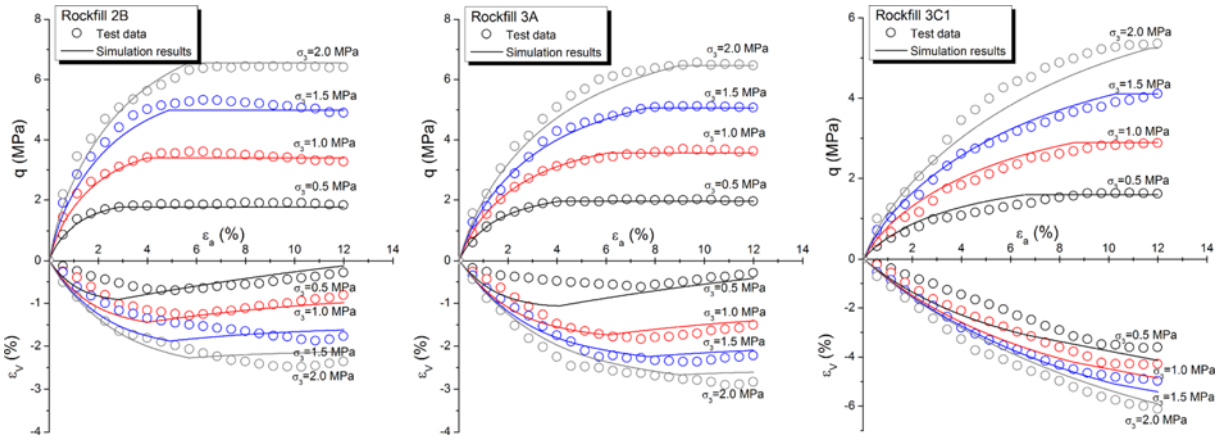

Fig. 7. Model Predictions and Triaxial Test Results for Nam Ngum 2 Rockfill Materials

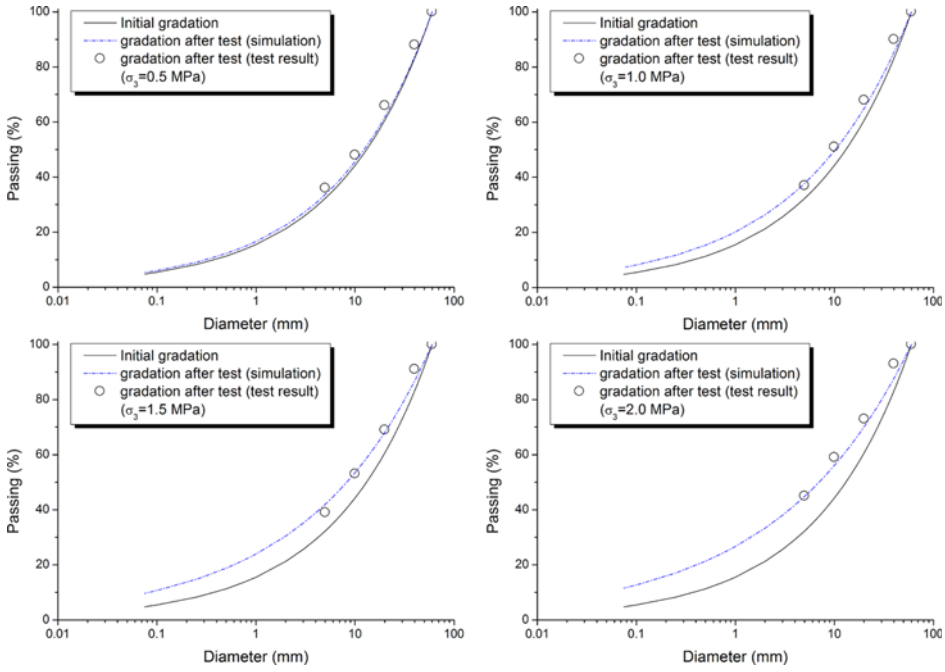

Fig. 8. Model Predictions and Particle Distribution Evolution for Various Confining Pressures (Type 3A)

the experimental data, as depicted in Fig. 8 (for type 3A). For the same parameter set, a comparison of the oedometer test data with the predicted results and the change in particle gradation after the test are shown in Figs. 9(a)-(b). As shown in these figures, the modified model can capture both the axial strain response ε_1 and the particle distribution after the test. Overall, in these comparisons, the predicted results are found to be consistent with the test results, especially in terms of the volumetric strain response.

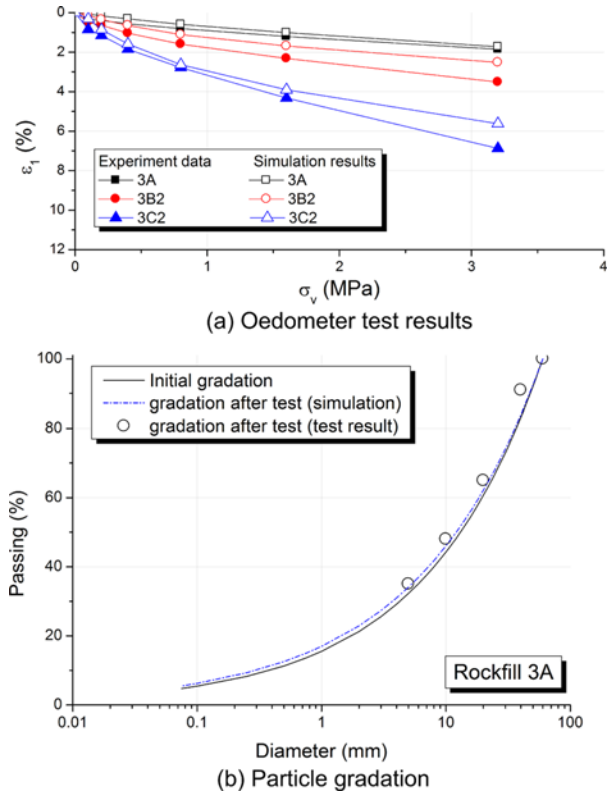

Fig. 9. (a) Model Predictions and Oedometer Test Results, (b) Model Predictions and Evolution of the Particle Distribution after the Test

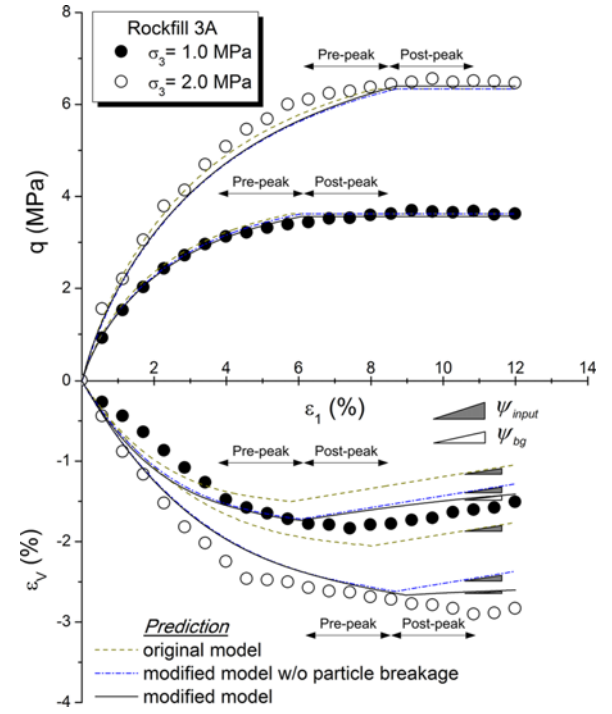

Fig. 10. Model Predictions for Different Values of *n/m* and Triaxial Test Results

Figure 10 compares the experimental results for rockfill 3A with those simulated using the original and modified models in terms of the stress-strain-volumetric strain curves. The results obtained from the modified model with and without particle breakage are included to illustrate the contribution of breakage. No significant difference among the simulations in terms of deviatoric stress is apparent. With regard to the volumetric strain response, it is clearly apparent that the modified model yields considerably improved predictions, especially the model that considers particle breakage. In the prediction generated by the modified model, the $\delta\varepsilon_v/\delta\varepsilon_1$ gradient (dilation) diminishes after the peak with an increasing degree of particle breakage (higher confining pressure), which is obviously observed in the case of a high confining pressure. Based on the outcomes, the consideration of particle breakage to suppress dilatancy appears reasonable.

5. Application of the Model for the Deformation Analysis of a High Rockfill Dam

5.1 Case Study

The Nam Ngum 2 (NN2) CFRD project is located on the Nam Ngum River in the Lao People's Democratic Republic, approximately 90 km north of the capital, Vientiane, and 35 km upstream of the Nam Ngum 1 dam and powerhouse. Table 2 summarizes

Table 2. General Characteristic of the Dam

Characteristics	Values	Unit
Dam Height	182	m
Crest elevation	381.00	m.asl.
Crest length	500	m
Crest width	9	m
Dam volume	9.7	million m^3
Concrete face slab area	88,000	m^2
Reservoir volume	4,900	million m^3

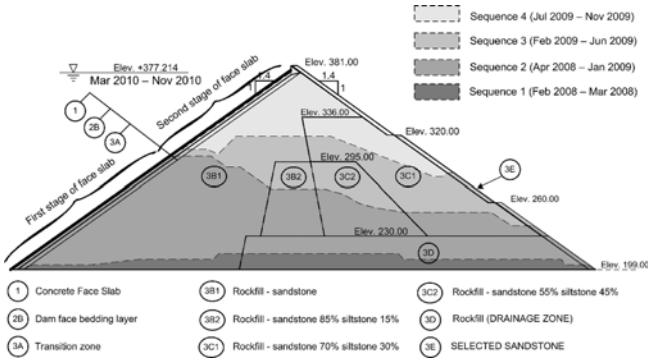

Fig. 11. Typical Section of the Nam Ngum 2 CFRD

the main characteristics of the NN2 CFRD. The designation of the CFRD rockfill zones follows the guidelines of the International Commission on Large Dams (ICOLD, 2004). The dam has an upstream slope of 1V : 1.4H (vertical : horizontal) and a downstream slope of 1V : 1.4H between the two berms (the slope is 1V : 1.5H including the berms).

Figure 11 illustrates the zoning of the dam, which consist of zone 1, which is the concrete face slab protection zone on the upstream side; zone 2B, the cushion zone; zones 3A, 3B1, 3C1, 3D and 3E, which are major rockfill zones; and finally, zones 3B2 and 3C2 (around the center of the dam), which are rockfill zones with high siltstone content. The thickness of the concrete face slab varies with the reservoir head, H (m):

$$\text{Face Slab Thickness, } T\text{ (m)} = 0.3 + 0.003H \quad (30)$$

The construction of the dam embankment was divided into four main sequences to correspond with the two stages of face slab construction. In Sequence 1, zones 3B1 and 3D were constructed, and the sequence was terminated at approximately 30 m from the toe. In Sequence 2, the dam embankment was constructed upstream until it reached an elevation of 293.4 m. The goal of this sequence was to prepare for the first stage of face slab construction. After the completion of the first stage of face slab construction, Sequence 3 was commenced near the central zone and downstream. The dam embankment construction completed at the end of Sequence 4, prior to the start of the second stage of face slab construction.

5.2 Finite Element Model

FEM is one of the available tools used in the prediction of CFRD behavior in terms of stresses and displacements. The earliest applications of FEM to model CFRDs were conducted under 2D plane strain conditions (e.g., Soroush and Araei, 2006; Zhou *et al.*, 2011; Xu *et al.*, 2012b). Under the narrow-valley condition for high CFRDs, a 2D deformation analysis would yield results that are not representative of reality because of the cross-valley arching effect (Giudici *et al.*, 2000; Znamensky, 2009). This necessitates modeling such a dam under 3D conditions. Figure 12(a) illustrates the 3D CFRD mesh used in this analysis. The dam body contained 105,758 4-node tetrahedral elements and 20,134 nodes. The boundary conditions were defined in terms of fixed displacements at the bottom and outer sides of the rock foundation, whose dimensions are 100×1000×1000 m (height× width×depth). The concrete face slab was modeled as a 3D shell element. The thicknesses of the shell elements were varied from 0.30 m at the dam crest to 0.843 m at the toe. The rock foundation and abutment were assumed to be linearly elastic, with a Young's modulus of 5.0 GPa and a Poisson's ratio of 0.2.

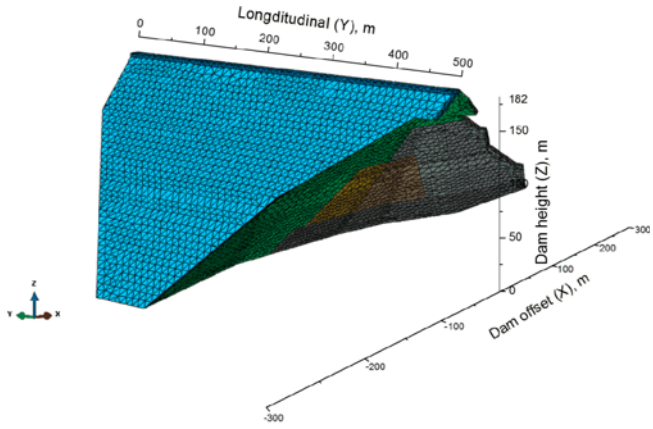

(a) 3D finite element mesh

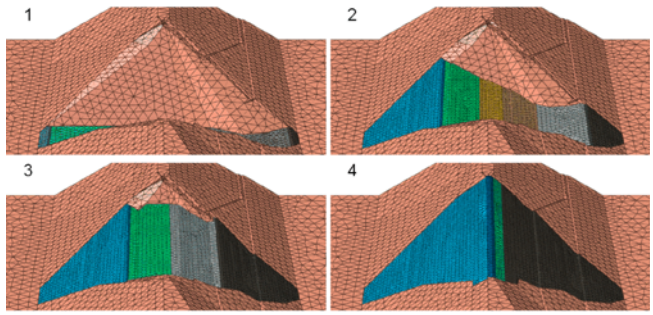

(b) stage of construction

Fig. 12. (a) Three-dimensional FE Model for the Analysis of the Nam Ngum 2 CFRD, (b) FE Stage of Construction

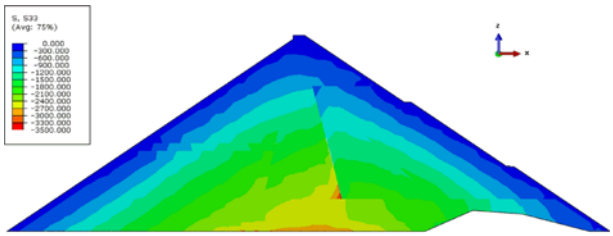

(a) Vertical stress distribution

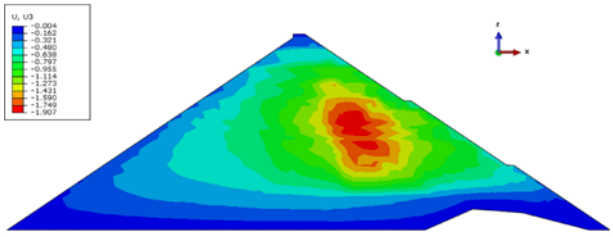

(b) Settlement contour

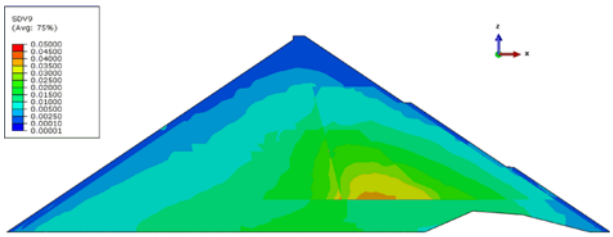

(c) Particle breakage

Fig. 13. Contours of the Predicted Results

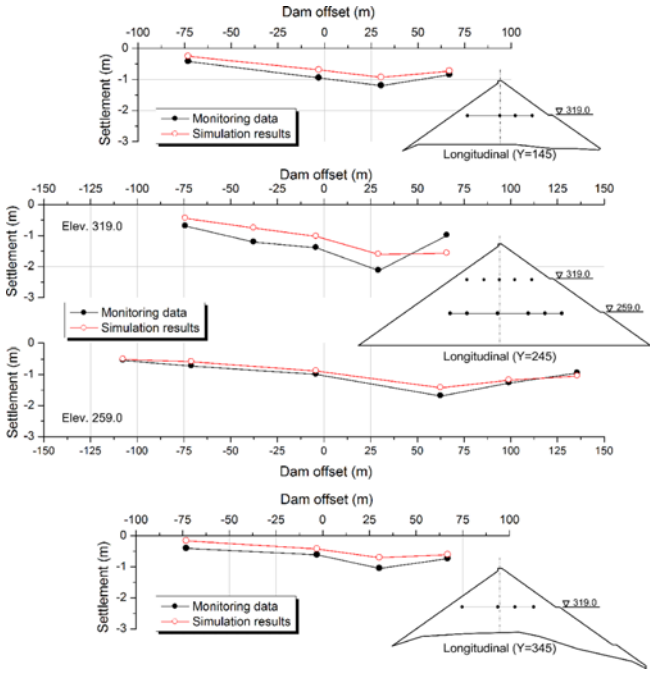

Fig. 14. The Predicted and Measured (using HSCs) Settlements

6. Analysis Results

The vertical stress contours are shown in Fig. 13(a). The maximum compressive stress occurs in the central zone, at an elevation of approximately 230 m.a.s.l. The maximum compressive stress lies in the range of 3500 kPa. The maximum settlement occurs in the rockfill in zones 3C1 and 3C2 (slightly downstream) because the overall stiffnesses of these zones are lower than those of the other zones, as seen in Fig. 13(b). The maximum measured settlement is approximately 1.9 m. Moreover, regarding particle breakage, simulations indicate an extent of particle breakage of approximately 4% (see Fig. 13(c)). Although the particle breakage is rather small, it nevertheless is not insignificant. For dams that have been newly constructed within the past decade, some of which have been built to over 200 m in height, the extent of particle breakage can exceed 10%. Therefore, the constitutive model used in the stress-deformation analysis of such rockfill dams should account for particle breakage behavior, particularly in the case of large dams.

The dam settlements were monitored using Hydraulic Settlement Cells (HSCs) and Settlement Gauges (SGs). Fig. 14 compares the predicted settlements and the results measured using the HSCs. The maximum settlement is observed in the deepest dam section (section 3) at an elevation of 319 m.a.s.l. The predicted results achieve satisfactory agreement with the field monitoring data, although slight under-prediction is apparent. The analysis results are consistent with previous publications (Zhou *et al.*, 2011; Jia and Chi, 2015) concerning the deformation analysis of the Shuibuya and Malutang 2 CFRDs. The calculated settlements (the model parameter determined from laboratory tests) are generally lower than the observed data. This may be attributed to the creep behavior of the rockfill materials, which has not been yet taken into consideration in this study. The settlements along the embankment height were monitored using sets of SGs in the downstream zone, as depicted in Fig. 15. Comparisons between the predicted results and the monitoring data indicate that the modified model is able to reasonably predict the settlement behaviors in the body of a high rockfill dam. The trends of the settlement profiles are reasonably well captured, and the computed magnitudes are generally in acceptable agreement with the observed data.

7. Conclusions

In this study, an elasto-plastic model with double yield surfaces,

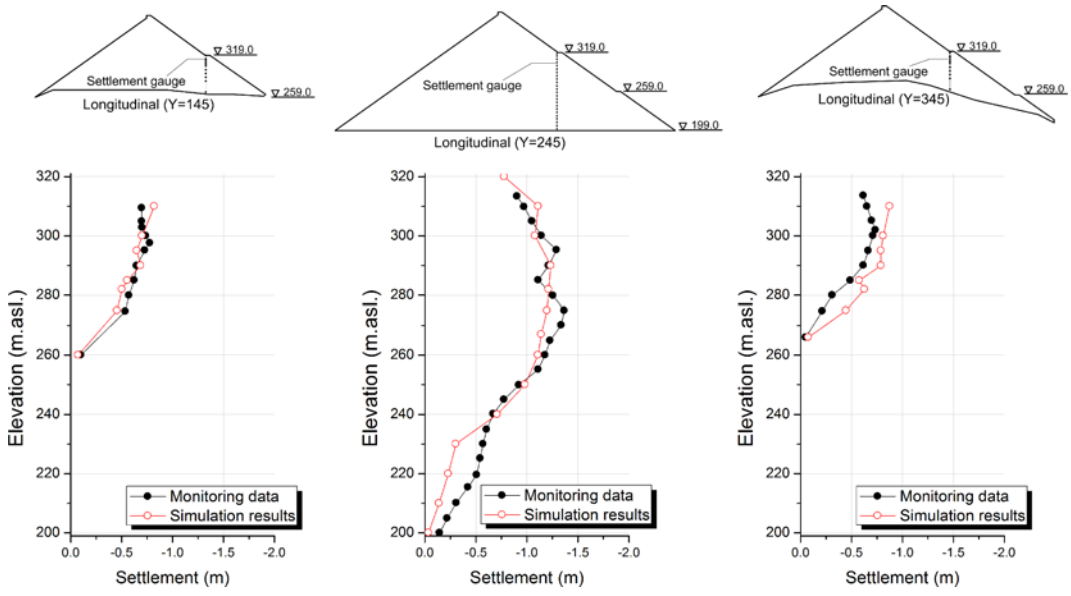

Fig. 15. The Predicted and Measured (using SGs) Settlements

into which many key features that reflect the behavior of rockfill materials had already been incorporated, was further developed for application to the deformation analysis of high rockfill dams. First, a preliminary investigation of the stress-dependent stiffnesses of rockfill under the stresses applied during triaxial and oedometer tests was performed, paying special attention to the degree of stress dependence. The findings of this investigation together with considerations of particle breakage were implemented in the modified model. To verify the performance of the developed constitutive model, the numerical responses under triaxial and oedometer testing conditions were simulated and compared with experimental results. Finally, the developed model was applied to predict the settlement of the Nam Ngum 2 CFRD during the construction stage. Based on the results reported in this study, the following conclusions can be drawn:

1. For rockfill materials, which are usually tested under high levels of stress, the volume change during shearing is strongly governed by the stress-dependent stiffness for primary compression. The degree of stress dependence for primary compression (n) is generally different from that for primary deviatoric loading (m).
2. For the specific types of rockfill materials considered in this study (blended sandstone and siltstone), the value of n is approximately 0.651 times the value of m.
3. Comparisons between model predictions and experimental test results show that by modifying the original model to include different degrees of evolution of the stress-dependent stiffness and particle breakage considerations, the developed constitutive model is endowed with the capability of capturing the stress-strain-volumetric strain change behavior of rockfill materials. The model predictions are in good agreement with both triaxial and oedometer testing data. The particle gradation predictions obtained using the proposed model reproduce the measured values reasonably well.
4. In the deformation analysis of a high CFRD, the results predicted at the observation points are in good agreement with the field data at the end of construction.

Acknowledgments

The authors gratefully acknowledge the financial support of the Thailand Research Fund (TRF) and King Mongkut's University of Technology Thonburi through the Royal Golden Jubilee Ph.D. program, under contract grant PHD/0006/2556. The authors also extend their appreciation to the Office of the Higher Education Commission for granting financial support through the Higher Education Research Promotion and National Research University (NRU) Project of Thailand. They are also indebted to the CK Power Public Company Limited and Nam Ngum 2 Power Company Limited for providing the valuable data.

References

Alonso, E. E., Olivella, S., Soriano, A., Pinyol, N. M., and Esteban, F. (2011). "Modelling the response of Lechago earth and rockfill dam." *Géotechnique*, Vol. 61, No. 5, pp. 387-407, DOI: 10.1680/geot.SIP11.P.013.

Araei, A. (2014). "Artificial neural networks for modeling drained monotonic behavior of rockfill materials." *International Journal of Geomechanics*, Vol. 14, No. 3, pp. 04014005, DOI: 10.1061/(ASCE)GM.1943-5622.0000323, 04014005.

Charles, J. A. and Watts, K. S. (1980). "The influence of confining pressure on the shear strength of compacted rockfill." *Géotechnique*, Vol. 30. No. 4, pp. 353-367, DOI: 10.1680/geot.1980.30.4.353.

Duncan, J. M. and Chang, C. Y. (1970). "Nonlinear analysis of stress-strain in soils." *Journal of the Soil Mechanics and Foundations Division*, ASCE, Vol. 96, No. 5, pp. 1629-1653.

Dunne, F. and Petrinic, N. (2005). *Introduction to computational plasticity*, Oxford University Press, Oxford.

Einav, I. (2007). "Breakage mechanics-Part II: Modelling granular materials." *Journal of the Mechanics and Physics of Solids*, Vol. 55, No. 6, pp. 1298-1320, DOI: 10.1016/j.jmps.2006.11.004.

Giudici, S., Herweynen, R., and Quinlan, P. (2000). "HEC experience in concrete faced rockfill dams-Past, present and future." *Proceedings of International Symposium on Concrete Faced Rockfill Dams, International Committee on Large Dams*, Beijing, China.

Hardin, B. O. (1987). "Crushing of soil particles." *Journal of Geotechnical Engineering*, Vol. 111, No. 10, pp. 1177-1192, DOI: 10.1061/(ASCE)0733-9410(1985)111:10(1177).

ICOLD (2004). "Concrete face rockfill dams: Concepts for design and construction 2004." *International Commission on Large Dams*, Paris, France.

IWHR (2007). *Report on laboratory tests of the rockfill materials of nam ngum 2 CFRD*. Institute of Water Resources and Hydropower Research, Beijing, China.

Jia, Y. and Chi, S. (2015). "Back-analysis of soil parameters of the Malutang II concrete face rockfill dam using parallel mutation particle swarm optimization." *Computers and Geotechnics*, Vol. 65, pp. 87-96, DOI: 10.1016/j.compgeo.2014.11.013.

Kohgo, Y., Takahashi, A., and Suzuki, T. (2010). "Evaluation method of dam behaviour during construction and reservoir filling and application to real dams." *Frontiers of Structural and Civil Engineering*, Vol. 4, Issue 1, pp. 92-101, DOI: 10.1007/s11709-010-0009-2.

Lade, P., Yamamuro, J., and Bopp, P. (1996). "Significance of particle crushing in granular materials." *Journal of Geotechnical and Geoenvironmental Engineering*, Vol. 122. Issue 4, pp. 309-316, DOI: 10.1061/(ASCE)0733-9410(1996)122:4(309).

Lee, K. L. and Farhoomand, I. (1967). "Compressibility and crushing of granular soil in anisotropic triaxial compression." *Canadian Geotechnical Journal*, Vol. 4, No. 1, pp. 68-86, DOI: 10.1139/t67-012.

Liu, H. and Zou, D. (2013). "Associated generalized plasticity framework for modeling gravelly soils considering particle breakage." *Journal of Engineering Mechanics*, Vol. 139, No. 5, pp. 606-615, DOI: 10.1061/(ASCE)EM.1943-7889.0000513.

Loupasakis, C. J., Christaras, B. G., Dimopoulos, G. Ch., and Hatzigogos, T. N. (2009). "Evaluation of plasticity models ability to analyze typical earth dams soil materials." *Geotechnical and Geological Engineering*, Vol. 27, No. 1, pp. 71-80, DOI: 10.1007/s10706-008-9212-5.

Mahabad, N. M., Imam, R., Javanmardi, Y., and Jalali, H. (2014). "Three-dimensional analysis of a concrete-face rockfill dam." *Proceedings of the ICE - Geotechnical Engineering*, Vol. 167, No. 4, pp. 323-343, DOI: 10.1680/geng.11.00027.

Marsal, R. J. (1967). "Large scale testing of rockfill materials." *Journal of Soil Mechanics and Foundation Engineering Division*, ASCE,

Vol. 93, No. SM2, pp. 27-43.

Miura, N. and O-Hara, S. (1979). "Particle-crushing of a decomposed granite soil under shear stresses." *Soils and Foundations*, Vol. 19, No. 3, pp. 1-14, DOI: 10.1016/0148-9062(80)90842-6.

NJHRI. (1999). *Specification of soil test (SL 237-1999)*, Ministry of Water Resources of the People's Republic of China, China Water Resources and Hydropower Press, Beijing.

Özkuzukiran, S., Özkan, M. Y., Özyazicioğlu, M., and Yildiz, G. S. (2006). "Settlement behaviour of a concrete faced rock-fill dam." *Geotechnical and Geological Engineering*, Vol. 24, pp. 1665-1678, DOI: 10.1007/s10706-005-5180-1.

Rowe, P. W. (1962). "The stress-dilatancy relation for static equilibrium of an assembly of particles in contact." *Proceedings of The Royal Society A*, Vol. 269, pp. 500-527.

Salim, W. and Indraratna, W. (2004). "A new elastoplastic constitutive model for coarse granular aggregates incorporating particle breakage." *Canadian Geotechnical Journal*, Vol. 41, No. 4, pp. 657-671, DOI: 10.1139/t04-025.

Schanz, T., Vermeer, P. A., and Bonnier, P. G. (1999). "The hardening soil model - formulation and verification." *Proceedings Plaxis Symposium* "*Beyond 2000 in Computational Geotechnics*", Amsterdam, Rotterdam, Balkema.

Soroush, A. and Araei, A. A. (2006). "Analysis of behaviour of a high rockfill dam." *Proceedings of the ICE - Geotechnical Engineering*, Vol. 159, No. 1, pp. 49-59, DOI: 10.1680/geng.2006.159.1.49.

Surarak, C., Likitlersuang, S., Wanatowski, D., Balasubramaniam, A., Oh, E., and Guan, H. (2012). "Stiffness and strength parameters for hardening soil model of soft and stiff Bangkok clays." *Soils and Foundations*, Vol. 52, No. 4, pp. 682-697, DOI: 10.1016/j.sandf.2012.07.009.

Varadarajan, A., Sharma, K., Venkatachalam, K., and Gupta, A. (2003). "Testing and modeling two rockfill materials." *Journal of Geotechnical and Geoenvironmental Engineering*, Vol. 129, No. 3, pp. 206-218, DOI: 10.1061/(ASCE)1090-0241(2003)129:3(206).

Varadarajan, A., Sharma, K. G., Abbas, S. M., and Dhawan, A. K. (2006). "Constitutive model for rockfill materials and determination of material constants." *International Journal of Geomechanics*, ASCE, Vol. 6, No. 4, pp. 226-237, DOI: 10.1061/(ASCE)1532-3641(2006) 6:4(226).

Xiao, Y., Liu, H., Chen, Y., and Jiang, J. (2014). "Strength and deformation of rockfill material based on large-scale triaxial compression tests. I: Influences of density and pressure." *Journal of Geotechnical and Geoenvironmental Engineering*, Vol. 140, No. 12, pp. 04014070, DOI: 10.1061/(ASCE)GT.1943-5606.0001176.

Xu, M. and Song, E. (2009). "Numerical simulation of the shear behavior of rockfills." *Computers and Geotechnics*, Vol. 36, No. 8, pp. 1259-1264, DOI:10.1016/j.compgeo.2009.05.010.

Xu, M., Song, E., and Chen, J. (2012a). "A large triaxial investigation of the stress-path-dependent behavior of compacted rockfill." *Acta Geotechnica*, Vol. 7, No. 3, pp. 167-175, DOI: 10.1007/s11440-012-0160-0..

Xu, B., Zou, J., and Liu, H. (2012b). "Three-dimensional simulation of the construction process of the Zipingpu concrete face rockfill dam based on a generalized plasticity model." *Computers and Geotechnics*, Vol. 43, pp. 143-154, DOI: 10.1016/j.compgeo.2012.03.002.

Yang, Z. Y. and Juo, J. L. (2001). "Interpretation of sieve analysis data using the box-counting method for gravelly cobbles." *Canadian Geotechnical Journal*, Vol. 38, No. 6, pp. 1201-1212, DOI: 10.1139/cgj-38-6-1201.

Znamensky, D. (2009). "Valleys shape influence on the volume safety factor and arch effect of high CFR recently built in brazil." *Commission Internationale des Grands Barrages*, Brasilia.

Zhang, G., Zhang, J. M., and Yu, Y. (2007). "Modeling of gravelly soil with multiple lithologic components and its application." *Soils and Foundations*, Vol. 47, No. 4, pp. 799-810, DOI: 10.3208/sandf.47.799.

Zhou, W., Hua, J., Chang, X., and Zhou, C. (2011). "Settlement analysis of the Shuibuya concrete-face rockfill dam." *Computers and Geotechnics*, Vol. 38, No. 2, pp. 269-280, DOI: 10.1016/j.compgeo.2010.10.004.